



PAPER • OPEN ACCESS

Investigation of degradation dynamics of 265 nm LEDs assisted by EL measurements and numerical simulations

To cite this article: Francesco Piva *et al* 2024 *Semicond. Sci. Technol.* **39** 075025

View the [article online](#) for updates and enhancements.

You may also like





- [High-output-power deep ultraviolet light-emitting diode assembly using direct bonding](#)
Masatsugu Ichikawa, Akira Fujioka, Takao Kosugi *et al.*
- [Uneven AlGaIn multiple quantum well for deep-ultraviolet LEDs grown on macrosteps and impact on electroluminescence spectral output](#)
Michiko Kaneda, Cyril Pernot, Yosuke Nagasawa *et al.*
- [Enhanced light extraction efficiency of UV LEDs by encapsulation with UV-transparent silicone resin](#)
Shaojun Wu, Martin Guttman, Neysha Lobo-Ploch *et al.*

247th ECS Meeting
Montréal, Canada
May 18-22, 2025
Palais des Congrès de Montréal

Showcase your science!

Abstracts due December 6th

Investigation of degradation dynamics of 265 nm LEDs assisted by EL measurements and numerical simulations

Francesco Piva^{1,*} , Matteo Buffolo¹, Nicola Roccatò¹, Marco Pilati¹, Simone Longato¹, Norman Susilo² , Daniel Hauer Vidal², Anton Muhin², Luca Sulmoni² , Tim Wernicke², Michael Kneissl^{2,3}, Carlo De Santi¹, Gaudenzio Meneghesso¹ , Enrico Zanoni¹ and Matteo Meneghini^{1,4}

¹ Department of Information Engineering, University of Padova, Padova, Italy

² Technische Universität Berlin, Institute of Solid State Physics, Berlin, Germany

³ Ferdinand-Braun-Institut (FBH), Berlin, Germany

⁴ Department of Physics and Astronomy, University of Padova, Padova, Italy

E-mail: francesco.piva@unipd.it

Received 31 January 2024, revised 22 May 2024

Accepted for publication 6 June 2024

Published 19 June 2024



Abstract

We studied four AlGaIn-based 265 nm LEDs with increasing QW thickness (1.4, 3, 6 and 9 nm) during a constant current stress at 100 A cm⁻². We focused our attention on the parasitic components of the emission spectra at low current levels and on the optical power recovery observed at high current levels. We associated every parasitic peak or band to a region in the device where they can be generated, also demonstrating if they are related to band-to-band emission or radiative emission through defects. At high current levels, we showed the simultaneous effect of the decrease in injection efficiency in the active region and the increase in non-radiative recombination, by fitting the EQE curves with a mathematical model. Moreover, we associated the optical power recovery with a generation of negative charge near the active region, which led to an increase in injection efficiency in the QW.

Keywords: parasitic emission, optical power recovery, UV-C LEDs

1. Introduction

AlGaIn-based ultraviolet (UV) light emitting diodes (LEDs) have gained an increasing interest in the last years for their use in disinfection systems [1–4]. In particular, it was

demonstrated that by UV light it is possible to inactivate several viruses, including Sars-CoV-2 [5]. This pushed the researchers to increase the external quantum efficiency (EQE), which is still about an order of magnitude lower than the visible LEDs [6]. These devices still suffer from: difficulties in the fabrication of p-contact [7, 8], since no metal can provide a good alignment with the valence band of (Al)GaIn; self-heating [6], caused by the low fraction of electrical power converted into optical power; low spectral purity [9], consequence of the presence of defects within the structures and of the heterostructure properties. Equally or even more important for real-life application is the stability of the output optical power, which is often overlooked. Consequently, only few studies

* Author to whom any correspondence should be addressed.



Original content from this work may be used under the terms of the [Creative Commons Attribution 4.0 licence](https://creativecommons.org/licenses/by/4.0/). Any further distribution of this work must maintain attribution to the author(s) and the title of the work, journal citation and DOI.

exist that investigate the degradation behavior of UV LEDs and the related physical processes.

The goal of this paper is to study the optical properties of single QW (SQW) LEDs, during an accelerated lifetime test (ALT). The devices under test are simplified structures, designed to ease the experimental evaluation of efficiency and lifetime limiting processes of AlGaIn-based UV-C emitters. Hence lifetime and EQE are not comparable with the performance reached by commercially-available devices. Despite that, these devices suffer from the same issues as their commercial counterpart, making them suitable for our investigation. We divided our study into two parts: a first part where we found the origin of the parasitic spectral components and a second where we investigated the mechanisms affecting the optical power at the stress current density. From the spectral analysis, we found two peaks related to band-to-band recombinations located at the interface between the p-contact layer (p-CL) and electron blocking layer (EBL) and at the interface between the interlayer (IL) and last barrier (LB). Moreover, we identified three peaks caused by defect recombination, generated in the p-CL, in the IL and in the QW or LB. Regarding the optical power at high current levels, i.e. at measurement currents near the stress current level, through mathematical simulations we confirmed the decrease in injection efficiency and the increase in non-radiative recombination as the main mechanisms of optical degradation. By means of TCAD simulations, carried out with Synopsys® Sentaurus, we were able to ascribe the optical recovery observed on the sample featuring thicker QWs to the screening of the polarization (PE) charge at the IL/LB interface, which led to an increase in carrier injection in the active region during the first 1000 min of ageing. A detailed description of the simulation approach and framework adopted for the same family of devices can be found in [10].

2. Experimental details

The devices under analysis are four sets of AlGaIn-based SQW LEDs, with a nominal emission wavelength of 265 nm. Their epitaxial structure, reported in figure 1, differs only in the QW thickness, which is 1.4, 3, 6 and 9 nm and they were named QW14, QW3, QW6 and QW9, respectively. The LEDs were grown by metal-organic vapor phase epitaxy on high-temperature annealed epitaxially laterally overgrown AlN on sapphire. The threading dislocation density detected for this template was $9 \times 10^8 \text{ cm}^{-2}$ [11, 12]; above this layer a series of adaptations layers were grown. Following them, the 200 nm $\text{Al}_{0.65}\text{Ga}_{0.35}\text{N}$ *n-contact layer* was grown, with a Si doping of $4 \times 10^{18} \text{ cm}^{-3}$. The n-side of the device was concluded with a 40 nm $\text{Al}_{0.65}\text{Ga}_{0.35}\text{N}$ *First Barrier* layer ([Si]: $5 \times 10^{18} \text{ cm}^{-3}$), the $\text{Al}_{0.48}\text{Ga}_{0.52}\text{N}$ SQW with different thickness and unintentional doped (u.i.d.), the 10 nm $\text{Al}_{0.63}\text{Ga}_{0.38}\text{N}$ LB u.i.d. layer and the 10 nm $\text{Al}_{0.82}\text{Ga}_{0.18}\text{N}$ u.i.d. IL. The p-side started with a 25 nm $\text{Al}_{0.75}\text{Ga}_{0.25}\text{N}$ EBL, doped with a Mg concentration of $1 \times 10^{19} \text{ cm}^{-3}$ and followed by the *p-Contact Layer* (p-CL), in GaN ([Mg]: $6 \times 10^{19} \text{ cm}^{-3}$).

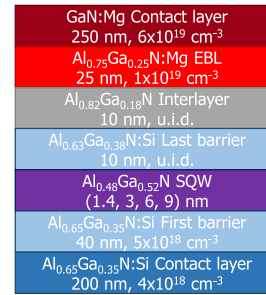


Figure 1. Schematic representation of the device's internal structure.

The devices were submitted to a constant current stress of 100 A cm^{-2} , which corresponded to the nominal current of 100 mA, at room temperature $25 \text{ }^\circ\text{C}$. Each test lasted 20 000 min, about 330 h and they were interrupted at logarithmic time steps to provide an electrical, optical and spectral characterization. The setup was composed of a source meter unit, a photodiode to measure the optical power and a calibrated compact array spectrometer to provide the spectral characterization at low current levels, i.e. for current levels below 10 mA. All measurements were performed in continuous wave mode. Before the ALTs, we also performed a detailed spectral analysis by a calibrated Instrument System CAS140, to evaluate the power spectral density (PSD) of the devices at all current levels.

3. Discussion

We started by investigating the emission spectra of the devices, as reported in figure 2(a) where is depicted the PSD of the QW3 LED. In the spectrum are visible several parasitic components, which are at least two orders of magnitude lower than the main peak at high current levels. In other words, at low current levels, parasitic emissions are comparable or higher than the characteristic 265 nm peak, resulting in the loss of the monochromaticity of the device. For these reasons, in our ALTs we investigated the evolution of the PSD at low current levels with time, as reported in the following section.

From the constant current ALTs, done in the same condition as our previous work [8], the optical power presented a degradation both at high and low current levels (figure 2(b)). First of all, from this graph, we can observe that a narrow QW implies a higher wavefunction overlap in it, leading to a higher emitted optical power. We already demonstrated that the decrease in optical power could be ascribed to an increase in non-radiative recombination events, possibly SRH [13, 14] and a decrease in injection efficiency [15, 16]. In particular, in this work, we decided to investigate two mechanisms that affect the optical power emission: (i) parasitic components at low current levels and (ii) recovery in optical power at high current levels.

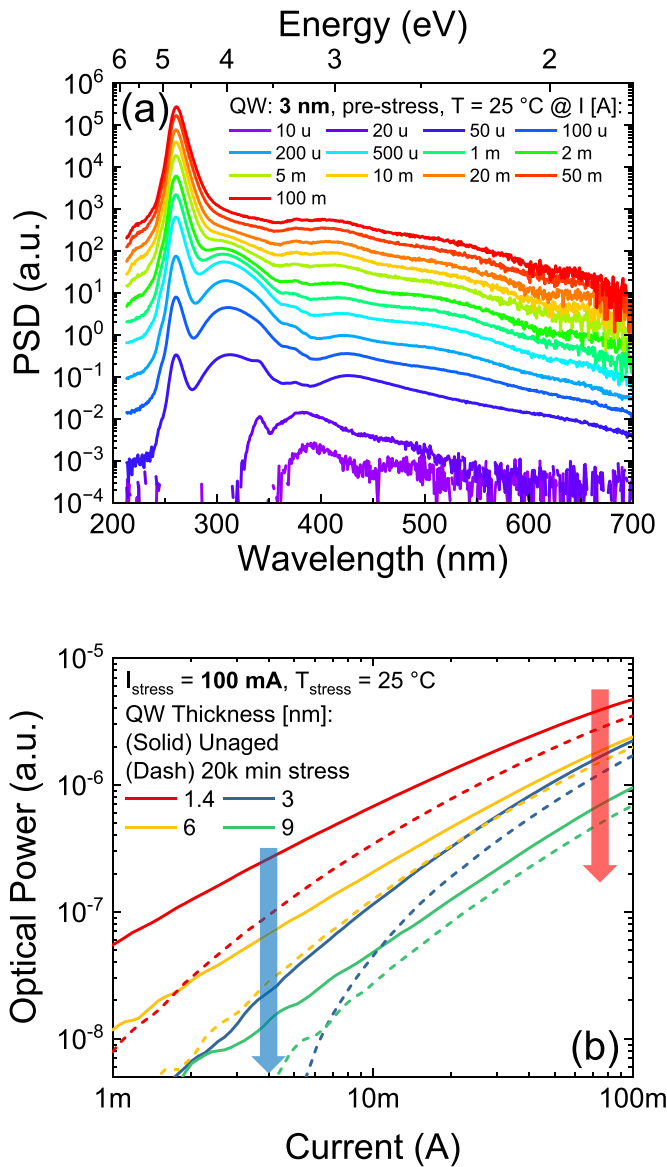


Figure 2. (a) Initial QW3 LED power spectral density characterization at various current levels. (b) LEDs absolute optical power before and after the stress.

3.1. PSD investigation at low current levels

Figure 3 reports the PSD of QW3 LED measured during the ageing procedure at the current level of 1 mA. As already discovered from the pre-stress characterizations, several parasitic peaks and bands are present besides the main peak. In particular, we identified: (i) a parasitic left-shoulder peak at 249 nm, (ii) a parasitic band at 308 nm, (iii) a parasitic peak at 337 nm, (iv) a parasitic band centered at 380 nm and (v) a parasitic band centered 506 nm. In table 1, we report the central wavelength of each peak or band extracted with a multiple Gaussian fit, the correspondent photon energy and the possible origin of the parasitic component (band-to-band recombination, or recombination through defects).

We aimed to identify the region in the device where each parasitic emission happened, so we divided the band diagram

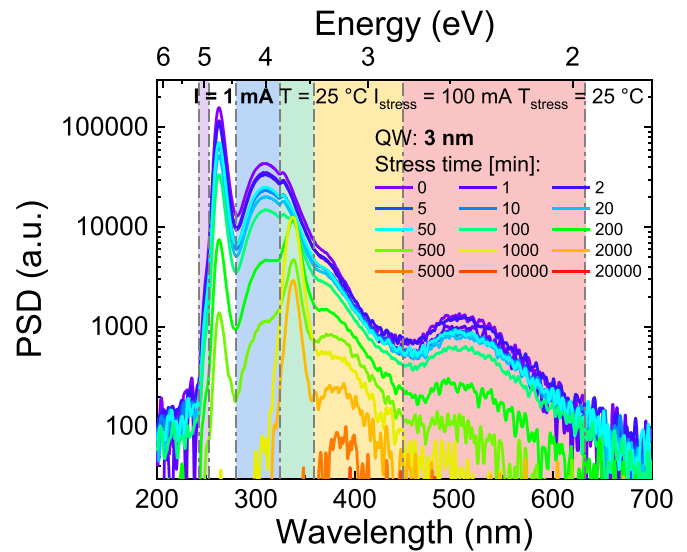


Figure 3. Power spectral density measured during the ageing procedure for the LED with QW of 3 nm. The colored background regions identify the wavelength ranges where each peak dominates.

as reported in figure 4(a). From these TCAD simulations, by analyzing the radiative recombination plot Bn^2 , we found an e^-/h^+ peak in correspondence to the QW, clearly associated to the main peak emission. Other carrier accumulation regions, which could give radiative recombination, are located at the interface between p-CL and EBL and between IL and LB. To validate our hypothesis, we also extracted the band diagram, by solving the Schrödinger equation, as reported in figure 4(b). This allowed us to identify four possible regions where we could have band-to-band recombination, in particular: (i) in the QW, with an emission energy of 4.6 eV, similar to the main emission peak; (ii) at the interface between IL and LB, with an emission energy of 4.90 eV, similar to component A; (iii) at the interface between EBL and IL, with an emission energy of 5.38 eV, for which we did not find any correspondence in figure 3; and (iv) at the interface between p-CL and EBL, with emission energy of 3.6 eV, similar to component D. It is worth noticing that the possible recombination at 5.38 eV has similar energy to the small peak present in the initial characterization at around 225 nm, visible only at high current levels. In fact, only at these current densities, we could accumulate a sufficient number of carriers to have band-to-band recombination. Moreover, to support the interpretation on the origin of peak A, photoluminescence analysis performed on similar UV LEDs confirmed the presence of a parasitic peak at 4.97 eV due to band-to-band recombination at the very same interface between IL and LB [17].

Continuing our investigation with the parasitic bands related to the recombination through defects, component F could be associated with the well-known GaN yellow luminescence band [18–21]. This allowed us to identify the p-CL in GaN (light-red background in figure 4(a)) as the candidate layer where this recombination happened.

Component E, with a peak energy of 3.26 eV, could be associated with a recombination through defects in the IL. In

Table 1. Summary of components identified in the power spectral density of device QW3.

Component	Wavelength (nm)	Energy (eV)	Physical origin	Location
A	249	4.97	Band-to-band	Interface between IL and LB
B	265	4.67	QW recomb.	Active region
C	308	4.03	Defects recomb.	Defects in QW or Mg back-diffusion in LB
D	337	3.68	Band-to-band	Interface between p-CL and EBL
E	380	3.26	Defects recomb.	Defects in LB or DAP in p-CL
F	506	2.45	Defects recomb.	GaN yellow luminescence in p-CL

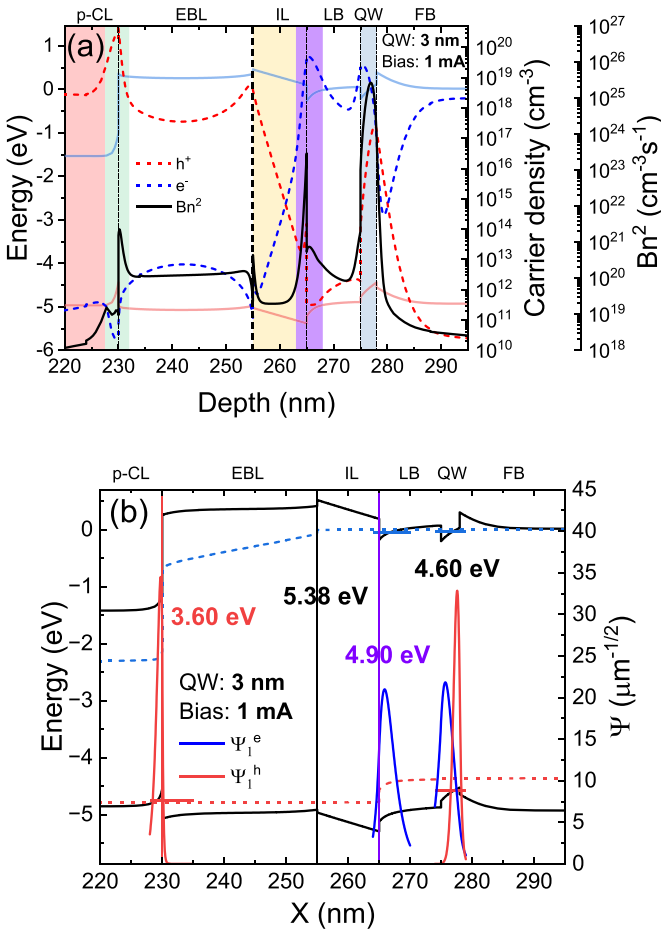


Figure 4. (a) TCAD simulation of the band diagram, carrier concentration and radiative recombination of QW3 LED at the current level of 1 mA. (b) Solution of the Schrödinger equation in the same conditions.

our previous work on the same samples [10], we provided a defect characterization with the DLOS technique, which allowed us to identify three deep levels at $E_C - 0.94$ eV, $E_C - 3.06$ eV and $E_C - 3.52$ eV. The second level had an activation energy similar to component E and it was also placed in the IL region to simulate the trap-assisted tunneling mechanism. By combining it with the high amount of carriers present at that interface, we could relate this parasitic band to the interface IL/LB, i.e. the region with a light-yellow background in figure 4(a). Another possible origin for the parasitic band E at 3.26 eV could be found in [22, 23], where the authors associated this band with recombination through a donor-acceptor

pair in a GaN layer, possibly driven by absorption and re-emission of higher energy light or electron overshoot. In this case, the peak could be generated on the p-side of the device, in the contact layer.

Concluding our investigation with component C, it could be related to recombination through defects present in the QW, as already reported in the literature [24]. Otherwise, another hypothesis could be a recombination in the LB through Mg defects back-diffused from the p-side during the growth. A similar behavior was already observed in [25], where the authors identified this level with a parasitic peak emission of about 280 nm.

In figure 5(a) we showed an important mechanism that appeared during the ageing procedure. After 1000 min of stress, the LED emission at low current levels is composed only of parasitic components, in particular by components D, E and partially F. These components are generated on the p-side of the device, in particular at the interface p-CL/EBL, in the IL and in the p-CL, respectively. This suggested the formation during the stress of a potential barrier at the interface LB/QW, possibly caused by a generation of positive charge, which locally bent the bands and reduced the injection efficiency in the active region. A similar behavior was already proposed in [8], where the authors modeled it to justify a decrease in injection efficiency observed during the ALT. In figure 5(b), we reported the normalized area of the PSD components in function of the stress time, to show how the peaks related to the n-side (A, B and C) went to zero after 500 min. As above mentioned, D, E and F keep appearing until 2000 min, when the non-radiative recombination prevailed zeroing the radiative emission.

3.2. Optical power recovery at high current levels

In figure 6(a), we report the optical power trends measured during the ALTs for the four LEDs in quasi-pulsed mode at the bias level adopted for the stress. We can observe the competition of two mechanisms: (i) a continuous optical power decay affecting the whole stress test, more evident in the device QW14 and (ii) a recovery in the optical power in the first 1000 min, which is higher for thicker QWs.

As mentioned at the beginning of section 3, the optical power reduction is supposed to be caused by a combination of two different processes: a decrease in injection efficiency and an increase in the non-radiative SRH recombination rate. To support this hypothesis, we mathematically reproduced the EQE curves of the QW14 device from the L-I characterization

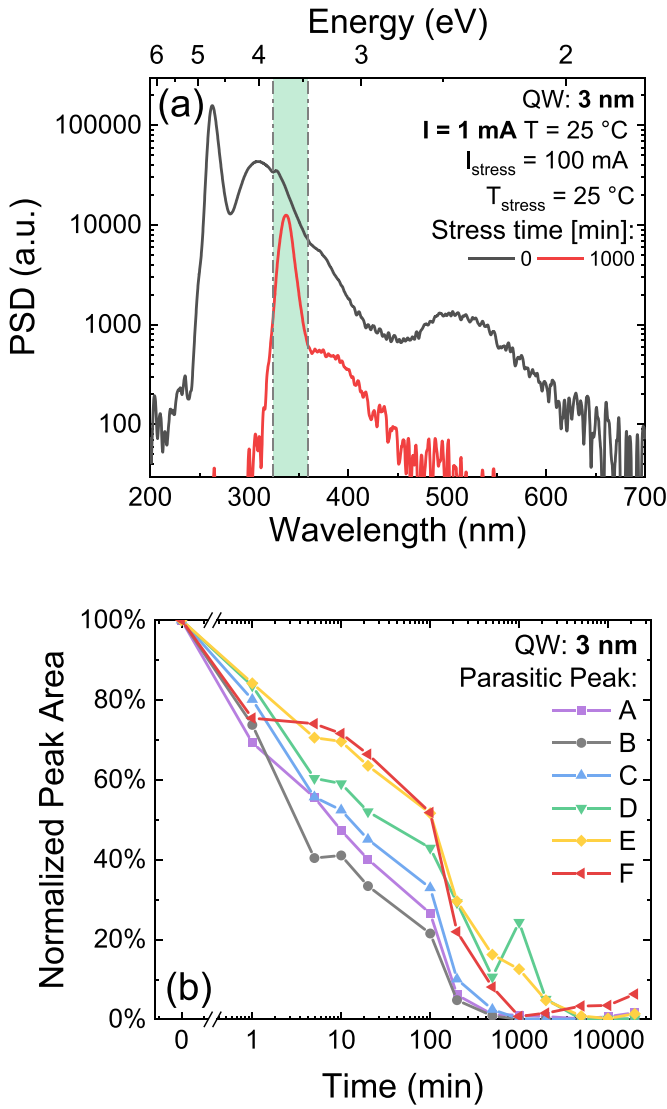


Figure 5. (a) Emission spectrum of QW3 LED at the beginning of the stress and after 1000 min. (b) Normalized area of the emission bands, calculated from the PSDs, during the stress test.

data. To this aim, we leveraged the conventional rate equation $\frac{dn}{dt} = \eta_{\text{inj}} \cdot \frac{I}{qV} - An - Bn^2 - Cn^3$, where q was the elementary charge, V the volume in the active region and I the current in the device. We chose the non-radiative (A), bimolecular (B) and Auger–Meitner (C) coefficients and the injection efficiency η_{inj} by starting from typical values reported in the literature for similar devices [26–28] and by reasonably adjusting them to fit the curves. The fitted curves reported in figure 6(b) were obtained by fixing the B and C coefficient, finding the values of A and η_{inj} that best fit the experimental curves at 0 min and by changing these latter two parameters to also fit the curve at 20 000 min. The plot showed that the sole increase in the A coefficient, i.e. an increase in defects-assisted SRH recombination, is not sufficient to reproduce the experimental curves, which also requires to take into consideration a decrease in injection efficiency. These results confirmed our hypotheses of a combination of an increase in non-radiative recombination

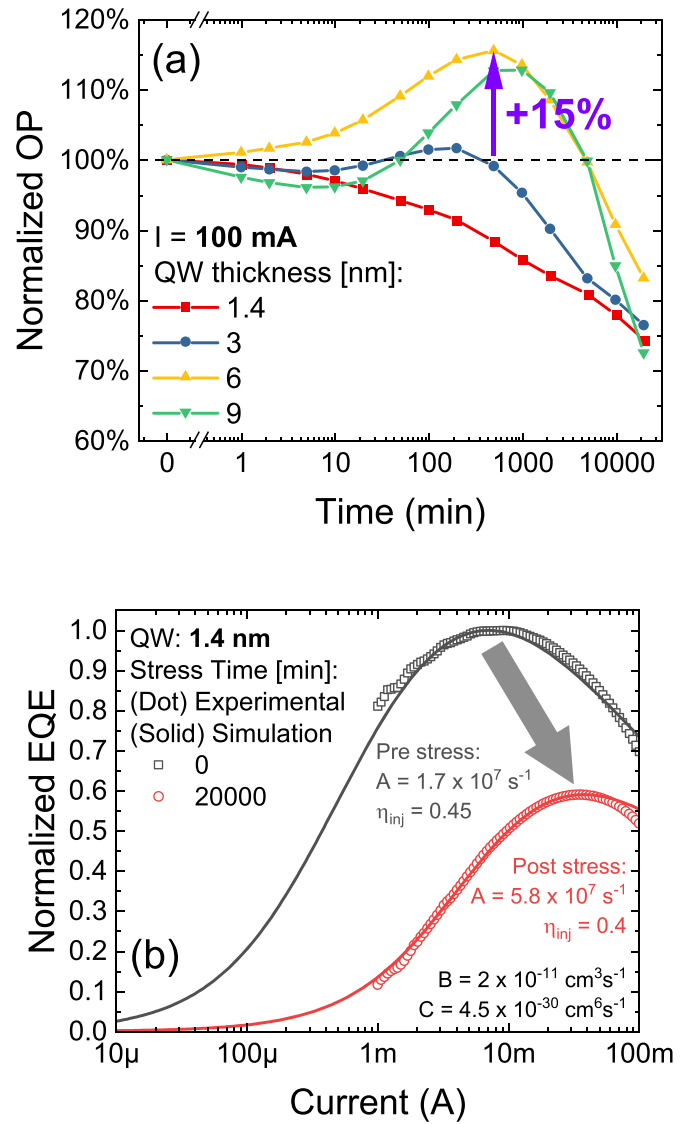


Figure 6. (a) Optical power trends normalized to the initial value at 0 min, at the stress current of 100 mA during the ageing. (b) Model of the EQE curve at the beginning and at the end of the stress for device QW14.

and a decrease in injection efficiency as the main mechanisms for the optical power degradation during ageing.

Regarding the optical power recovery, it was found to be more prominent for thicker QWs, reaching 15% for the 6 nm variant. To explain this mechanism, we hypothesized the formation of a negative charge at the interface between the IL and the LB (IL/LB), with the effect of screening the (positive) PE charge present there. We estimated the initial value of this fixed interface charge (IC) density in about 1×10^{11} cm $^{-2}$. Through our simulations, we demonstrated that this process can induce a rise of the valence band (see the inset of figure 7(b)), which led to a higher hole injection probability and consequently an increase in the main radiative recombination peak, as shown in figure 7(a). This increase could easily reach 15% of the initial value (figure 7(b)), supporting our hypothesis about the generation of negative charge at the interface during the first

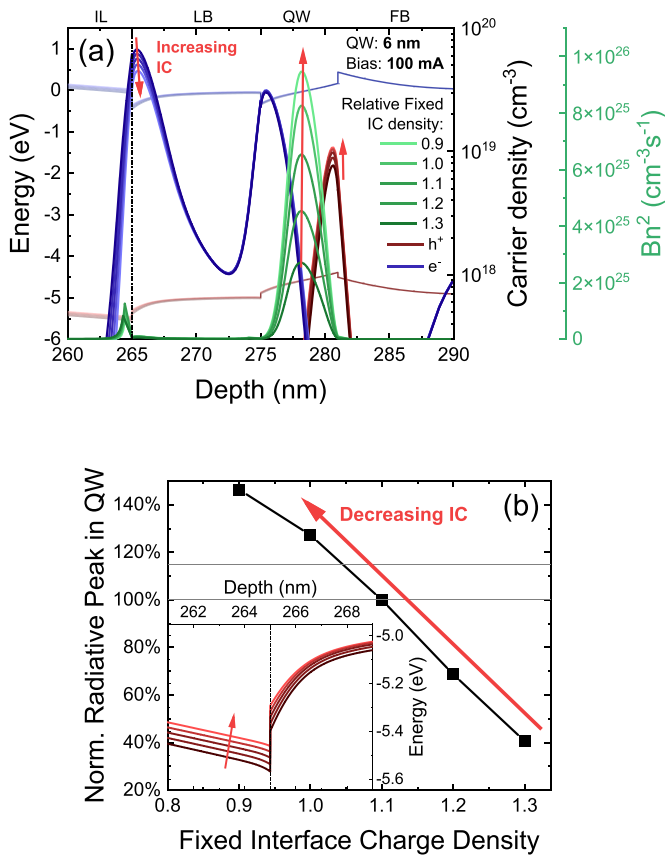


Figure 7. (a) Simulations of carrier density and radiative recombination in device QW6, with a decreasing PE charge at the IL/LB interface. (b) Normalized radiative recombination peak into the QW in function of the fixed IC charge; in the inset a zoom of the valence band at the interface IL/LB.

1000 min of stress. Defects acting as charged centers can therefore impact the optical characteristics of UV-C LEDs inducing a local band bending, which leads to an increase in hole injection efficiency and then an increase in radiative recombination in the QW. To confirm this preliminary hypothesis, further experiments, simulations and analyses are required.

4. Conclusions

In this paper, we presented an extensive study of the spectral impurities and the optical power degradation mechanisms of a series of AlGaIn-based SQW LEDs. We correlated the presence of two parasitic peaks to a band-to-band recombination that occurs at the interfaces IL/LB and p-CL/EBL, with emission wavelengths of about 249 and 337 nm, respectively. We also identified three parasitic bands, generated by recombination through defects, at 308, 380 and 506 nm, which took place in the active region, IL or p-CL and p-CL, respectively. Regarding the degradation mechanisms that reduced the optical power during ageing, we confirmed the simultaneous effect of an increase in non-radiative recombination and a decrease in injection efficiency. Meanwhile, we explained the optical recovery with a generation of negative charge at

the IL/LB interface, which increased the injection efficiency in the active region.

Data availability statement

The data cannot be made publicly available upon publication due to legal restrictions preventing unrestricted public distribution. The data that support the findings of this study are available upon reasonable request from the authors.

Acknowledgments

Project funded under the National Recovery and Resilience Plan (NRRP), Mission 4, Component C2, Investment 1.1, by the European Union—NextGenerationEU. PRIN Project 20225YYLEP, ‘Empowering UV Led technologies for high-efficiency disinfection: from semiconductor-level research to SARs-Cov-2 inactivation’.

ORCID iDs

Francesco Piva  <https://orcid.org/0000-0003-3620-5510>
 Norman Susilo  <https://orcid.org/0000-0002-5583-629X>
 Luca Sulmoni  <https://orcid.org/0000-0002-5341-7032>
 Gaudenzio Meneghesso  <https://orcid.org/0000-0002-6715-4827>

References

- [1] Kowalski W J 2020 2020 COVID-19 coronavirus ultraviolet susceptibility (PurpleSun) pp 1–4
- [2] Soler M, Scholtz A, Zeto R and Armani A M 2020 Engineering photonics solutions for COVID-19 *APL Photonics* **5** 090901
- [3] Glaab J et al 2021 Skin tolerant inactivation of multiresistant pathogens using far-UVC LEDs *Sci. Rep.* **11** 1–11
- [4] Piva F, Buffolo M, De Santi C, Meneghesso G, Zanoni E, Meneghini M and Trivellin N 2023 Status of performance and reliability of 265 nm commercial UV-C LEDs in 2023 *IEEE Trans. Electron Devices* **70** 5696–700
- [5] Trivellin N et al 2021 Uv-based technologies for sars-cov2 inactivation: status and perspectives *Electronics* **10** 1703
- [6] Amano H et al 2020 The 2020 UV emitter roadmap *J. Phys. D: Appl. Phys.* **53** 503001
- [7] Lee K, Bharadwaj S, Protasenko V, Xing H G and Jena D 2019 Efficient InGaIn p-contacts for deep-UV light emitting diodes *Device Research Conf. (DRC)* vol 2019 pp 171–2
- [8] Piva F et al 2023 Degradation of AlGaIn-based UV-C SQW LEDs analyzed by means of capacitance deep-level transient spectroscopy and numerical simulations *Appl. Phys. Lett.* **122** 181102
- [9] Trivellin N, Monti D, Piva F, Buffolo M, De Santi C, Zanoni E, Meneghesso G and Meneghini M 2019 Degradation processes of 280 nm high power DUV LEDs: impact on parasitic luminescence *Jpn. J. Appl. Phys.* **58** SCCC19
- [10] Roccato N et al 2023 Modeling the electrical degradation of AlGaIn-based UV-C LEDs by combined deep-level optical spectroscopy and TCAD simulations *Appl. Phys. Lett.* **122** 161105
- [11] Enslin J, Knauer A, Mogilatenko A, Mehnke F, Martens M, Kuhn C, Wernicke T, Weyers M and Kneissl M 2019 Determination of sapphire off-cut and its influence on the

- morphology and local defect distribution in epitaxially laterally overgrown AlN for optically pumped UVC lasers *Phys. Status Solidi a* **216** 1900682
- [12] Susilo N *et al* 2020 Improved performance of UVC-LEDs by combination of high-temperature annealing and epitaxially laterally overgrown AlN/sapphire *Photon. Res.* **8** 589
- [13] Piva F *et al* 2020 Defect incorporation in In-containing layers and quantum wells: experimental analysis via deep level profiling and optical spectroscopy *J. Appl. Phys.* **54** 7
- [14] Ruschel J, Glaab J, Mahler F, Kolbe T, Einfeldt S and Tomm J W 2020 In-situ spectroscopic analysis of the recombination kinetics in UVB LEDs during their operation *Appl. Phys. Lett.* **117** 121104
- [15] Rozhansky I V and Zakheim D A 2006 Analysis of dependence of electroluminescence efficiency of AlInGaN LED heterostructures on pumping *Phys. Status Solidi c* **3** 2160–4
- [16] Piva F, De Santi C, Deki M, Kushimoto M, Amano H, Tomozawa H, Shibata N, Meneghesso G, Zanoni E and Meneghini M 2020 Modeling the degradation mechanisms of AlGaIn-based UV-C LEDs: from injection efficiency to mid-gap state generation *Photon. Res.* **8** 1786
- [17] Susilo N *et al* 2018 AlGaIn-based deep UV LEDs grown on sputtered and high temperature annealed AlN/sapphire *Appl. Phys. Lett.* **112** 41110
- [18] Calleja E *et al* 1997 Yellow luminescence and related deep states in undoped GaN *Phys. Rev. B* **55** 4689–94
- [19] Arslan E, Bütün S, Lisesivdin S B, Kasap M, Ozcelik S and Ozbay E 2008 The persistent photoconductivity effect in AlGaIn/GaN heterostructures grown on sapphire and SiC substrates *J. Appl. Phys.* **103** 103701
- [20] Neugebauer J and Van de Walle C G 1996 Gallium vacancies and the yellow luminescence in GaN *Appl. Phys. Lett.* **69** 503–5
- [21] Reshchikov M A 2021 Measurement and analysis of photoluminescence in GaN *J. Appl. Phys.* **129** 121101
- [22] Paskova T, Arnaudov B, Paskov P P, Goldys E M, Hautakangas S, Saarinen K, Södervall U and Monemar B 2005 Donor-acceptor pair emission enhancement in mass-transport-grown GaN *J. Appl. Phys.* **98** 33508
- [23] Krishna S Aggarwal N, Gundimeda A, Sharma A, Husale S, Maurya K K and Gupta G 2019 Correlation of donor-acceptor pair emission on the performance of GaN-based UV photodetector *Mater. Sci. Semicond. Process.* **98** 59–64
- [24] Polyakov A Y, Smirnov N B, Govorkov A V, Kozhukhova E A, Dabiran A M, Chow P P, Wowchak A M, Lee I-H, Ju J-W and Pearton S J 2009 Comparison of electrical properties and deep traps in p Al_xGa_{1-x}N grown by molecular beam epitaxy and metal organic chemical vapor deposition *J. Appl. Phys.* **106** 073706
- [25] Nakarmi M L, Nepal N, Lin J Y and Jiang H X 2009 Photoluminescence studies of impurity transitions in Mg-doped AlGaIn alloys *Appl. Phys. Lett.* **94** 091903
- [26] Muhiin A *et al* 2022 Radiative recombination and carrier injection efficiencies in 265 nm deep UV LEDs grown on AlN/sapphire templates with different defect densities *Phys. Status Solidi a* **220** 2200458
- [27] Nippert F, Tollabi Mazraehno M, Davies M J, Hoffmann M P, Lugauer H-J, Kure T, Kneissl M, Hoffmann A and Wagner M R 2018 Auger recombination in AlGaIn quantum wells for UV light-emitting diodes *Appl. Phys. Lett.* **113** 071107
- [28] Ishii R, Yoshikawa A and Nagase K 2020 Temperature-dependent electroluminescence study on 265-nm AlGaIn-based deep-ultraviolet light-emitting diodes grown on AlN substrates *AIP Adv.* **10** 125014